OPEN ACCESS

Environment & Ecology ARTICLE

The Innovation Geoscience

Canopy structure–biomass coupling strengthens with age under stage-dependent environmental controls during China's forest recovery

Kai Cheng,[1] Ang Chen,[1] Yixuan Zhang,[1] and Qinghua Guo[1,2,*]

*Correspondence: guo.qinghua@pku.edu.cn

Received: December 3, 2025; Accepted: May 8, 2026; Published Online: May 11, 2026; https://doi.org/10.59717/j.xinn-geo.2026.100228

GRAPHICAL ABSTRACT

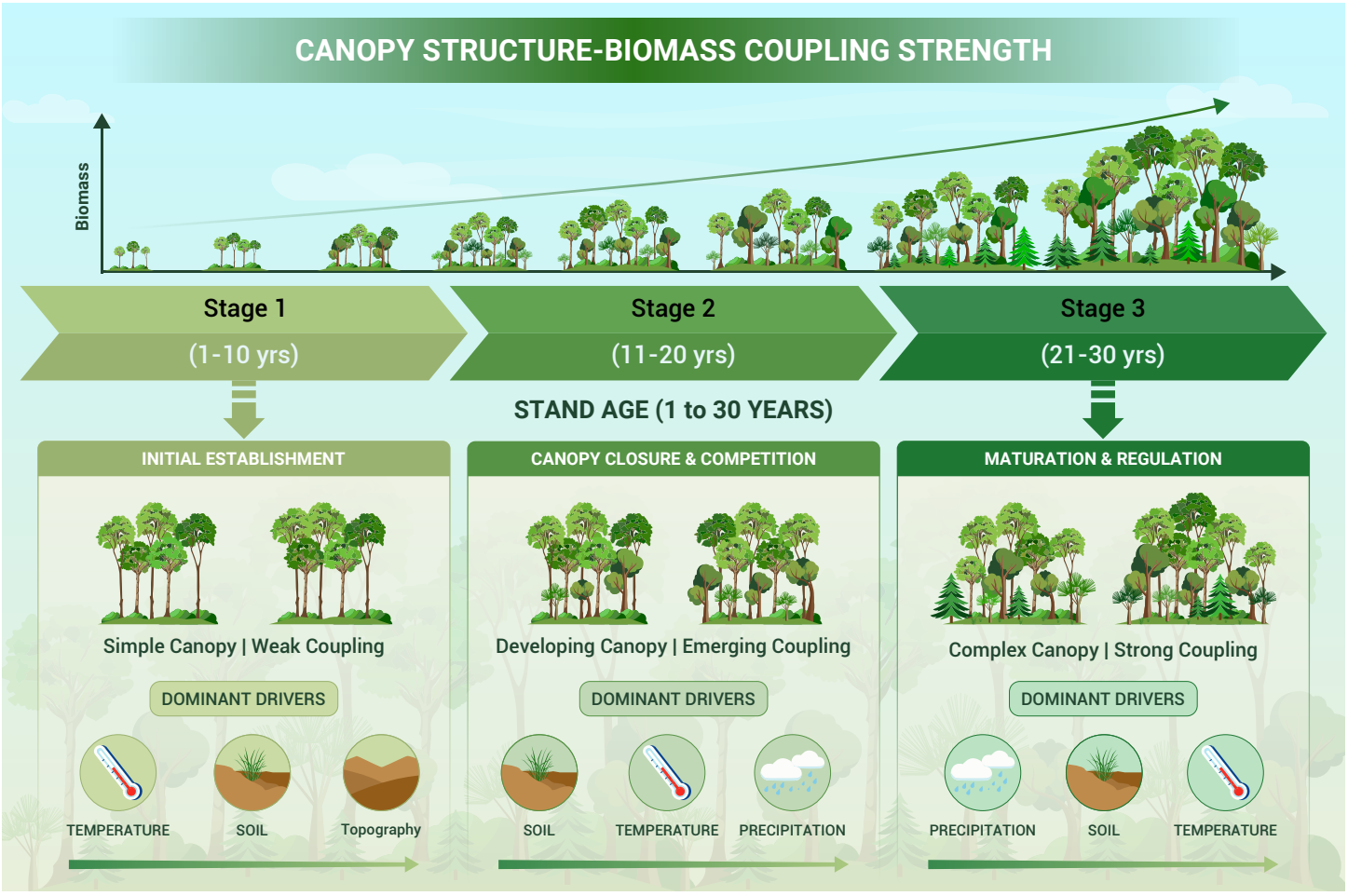

PUBLIC SUMMARY

- Stand age significantly strengthens the coupling of canopy structural complexity and biomass density.
- Early-established structural fingerprints provide stable, biome-specific benchmarks for recovery.
- Forest structure recovery drivers shift dynamically from temperature, to soil, and precipitation.

ARTICLE Environment & Ecology

OPEN ACCESS

Canopy structure–biomass coupling strengthens with age under stage-dependent environmental controls during China's forest recovery

Kai Cheng,[1] Ang Chen,[1] Yixuan Zhang,[1] and Qinghua Guo[1,2,*]

[1]Institute of Remote Sensing and Geographic Information System, School of Earth and Space Sciences, Peking University, Beijing 100087, China

[2]Institute of Ecology, College of Urban and Environmental Sciences, Peking University, Beijing 100087, China

*Correspondence: guo.qinghua@pku.edu.cn

Received: December 3, 2025; Accepted: May 8, 2026; Published Online: May 11, 2026; https://doi.org/10.59717/j.xinn-geo.2026.100228

Citation: Cheng K., Chen A., Zhang Y., et al. (2026). Canopy structure–biomass coupling strengthens with age under stage-dependent environmental controls during China's forest recovery. *The Innovation Geoscience* **4**:100228.

Forest restoration is a critical nature-based solution, yet our understanding of its structural development often relies on static, universal assumptions. This study challenges that paradigm by revealing the dynamic, context-dependent principles of forest recovery. By integrating multisource remote sensing data over China's 30-year period of natural forest regeneration, we find that the positive coupling between canopy structural complexity and aboveground biomass strengthens significantly with stand age. We found that distinct forest biomes exhibit unique structural fingerprints that are established early and persist through early restoration. Crucially, these recovery pathways are characterized by a predictable shift in dominant environmental drivers: from initial filtering mainly by temperature to mid-stage limitation by soil resources, and finally to regulation by precipitation in more mature stands. This work presents a dynamic framework for establishing biome-specific restoration targets and developing adaptive management strategies to increase global ecosystem resilience.

INTRODUCTION

As a nature-based solution, forest restoration plays a crucial role in addressing climate change and protecting biodiversity.[1-5] Therefore, a global call to protect forests and increase their quantity and quality exists;[1] however, monitoring and predicting the overall effectiveness of these nature-based solutions across vast, heterogeneous landscapes remains a significant scientific challenge. While traditional field surveys can provide crucial data on structural and diversity parameters such as diameter at breast height, tree height, species diversity, and richness, the limited coverage and representativeness of field plots restrict our ability to accurately capture large-scale ecosystem dynamics.[6-12] Consequently, bridging this monitoring gap using scalable indicators is essential to accurately assess the true efficacy of nature-based solutions and to ensure they deliver the promised climate and biodiversity benefits.

In recent years, ecosystem structural variables derived from remote sensing data have enabled the assessment of the effectiveness of large-scale restoration programs in a more feasible, efficient, and cost-effective manner.[13] Among them, canopy structural complexity (CSC), specifically quantified as canopy entropy, offers distinct advantages over traditional metrics such as canopy cover, foliage height diversity, canopy top rugosity, and fractal dimension.[14] Unlike dimensional metrics that focus on external boundaries, canopy entropy accounts for the complexity of the canopy structure in both vertical and horizontal dimensions.[15] By quantifying the thermodynamic disorder of return energy within the lidar waveform, canopy entropy directly reflects the complexity of light interception and niche partitioning processes that continue to evolve long after canopy closure.[14] Therefore, in the context of forest recovery, canopy entropy provides a more sensitive and comprehensive indicator of the transition from simple, single-layered cohorts to complex, multi-layered mature forests compared to traditional dimensional metrics.[16,17]

Many previous studies have suggested that forests with more complex structures have higher productivity and greater carbon storage capacity,[18] primarily because complex canopies can support higher biomass densities by optimizing light-capture efficiency and space-use efficiency.[19,20] This positive structure-function relationship has been validated in numerous studies across various scales.[17,18] However, most studies have revealed this relationship from a static perspective, overlooking a crucial issue: forest restoration is a dynamic, decades-long succession process. Therefore, does this fundamental structure-function relationship remain consistent throughout the entire restoration process? For instance, in the early stages of recovery, forests dominated by fast-growing, light-demanding species may prioritize rapid vertical growth. This process could fundamentally alter the nature of this scaling relationship, distinguishing it from mature forests regulated by gap dynamics and complex stratified structures.[21-25] This suggests that the scaling exponent linking structure and function is a dynamic variable that evolves across recovery stages. To date, corresponding research on time series tests of this ecological principle at the continental scale is lacking.

Moreover, this structural recovery trajectory is unlikely to be uniform. Natural forests inherently possess complexity and comprise diverse biomes.[26] Each biome is shaped by its unique evolutionary history and environmental context.[27] From moist, species-rich tropical and subtropical forests to cold-adapted, resilient boreal forests, the pathways of structural recovery are expected to vary significantly.[28] This finding raises a key question: Do different forest biomes exhibit distinct structural patterns at similar stages of recovery? Establishing such context-dependent baselines is crucial for moving beyond "one-size-fits-all" restoration approaches. These baselines enable us to set biome-specific recovery targets and more accurately assess restoration progress. Without comprehensive continental-scale assessments, our understanding of forest recovery remains fragmented and biased by studies from a limited number of ecosystems.

These potential divergent recovery pathways further raise a mechanistic question: What environmental drivers underlie the formation of these different structures? Although climate, topography, and soil properties have been shown to influence the forest structure, their relative importance may change systematically as the forest develops. For example, in young, recovering forests, soil nutrients may be the main bottleneck for structural development, whereas in mature, stable systems, water availability or extreme temperatures may become the dominant limiting factor.[29-31] Uncovering these shifting control factors is the key to moving from descriptive patterns to predictive, process-based models. A systematic quantification of these context-dependent environmental drivers across successional time and different biomes is lacking.

This study leverages the extensive forest restoration in China over the past three decades as a representative natural experiment to address the aforementioned fundamental questions. This unique context spans multiple climate zones and encompasses various forest types at different stages of natural recovery,[26] providing an unparalleled opportunity to dissect the dynamic processes of structural restoration. By integrating multisource remote sensing data, we adopted a "space-for-time" approach to construct a comprehensive spatiotemporal view of the canopy structure.[32-34] While we acknowledge the inherent assumptions of this method,[34] it provides an unparalleled opportunity to dissect the dynamic processes of structural maturation at a continental scale. Specifically, we first examined the universality of scaling relationships between CSC and biomass across different recovery stages. Next, we quantified the unique structural fingerprints of China's major forest biomes during restoration. Here, we define the structural fingerprint as the characteristic, biome-specific trajectory of CSC accumulation over time, specifically including two distinct dimensions: (1) the magnitude of complexity specific to each recovery stage, and (2) the temporal persistence of relative differences among biomes. Finally, and most crucially, we revealed the shifting combinations of environmental factors that drive

structural development, demonstrating that dominant controls depend simultaneously on both the forest biome and the recovery stage.

MATERIALS AND METHODS

Natural forest recovery dataset

The spatial and age distribution data obtained during natural forest restoration form the foundation of our research. The data were collected in our previous research and are based on Landsat image collections and time series change detection algorithms. The temporal accuracy of this data has been rigorously validated using independent field samples, achieving an R^2 of over 0.7.[28] For detailed production processes, please refer to our earlier study.[28] These data depict the extent of forests that have been reverted to natural forests through restoration since 1990 and remained so in 2020, along with their corresponding ages, at a spatial resolution of 30 m (Figure S1A).

Canopy structural complexity dataset

We quantified the structural complexity of these restored natural forests using the canopy entropy metric, which has been suggested as an effective index for quantifying forest canopy structural complexity and successfully captures the characteristics of canopy structural variation.[33] Compared with traditional metrics such as the widely used indicators canopy cover, foliage height diversity, canopy top roughness, and fractal dimension, this indicator overcomes common limitations, including susceptibility to saturation in structurally complex stands and insufficient reflection of internal canopy structural variations, demonstrating superior performance.[14] Moreover, this indicator has been shown to be significantly positively correlated with global forest productivity and stability,[17] making it an ideal comprehensive indicator for measuring the recovery of forest ecological functions. In this study, the method and parameters established by Liu et al.[17] were employed based on Global Ecosystem Dynamics Investigation (GEDI) lidar L2B data, which was originally designed and validated for global-scale applications. To strictly ensure the reliability of the structural metrics and minimize waveform artifacts, we applied rigorous algorithm-level quality filters directly to the GEDI L2B data. Specifically, we exclusively retained high-quality observations by requiring sensitivity > 0.9, l2_quality_flag = 1, and degrade_flag = 0. In total, we obtained canopy structural complexity data spanning the entire study area (Figure 2A), comprising 1,568,725 footprints at a 25 m spatial resolution.

Ecosystem function dataset

We selected aboveground biomass density (AGBD) as the primary indicator of ecosystem function, specifically representing the forest's capacity for carbon storage. The AGBD data were sourced from the L4A product of the GEDI (version 2.1), which provides high-quality footprint-scale AGBD data (Mg ha-1) with a spatial resolution of 25 m. These data have been extensively applied and validated in AGB mapping at national, regional, and global scales.[36] For this study, we extracted all AGBD data from 2020 that spatially overlapped the study area for analysis and modeling (Supplementary Figure 1B).

Environmental variables

We compiled a comprehensive suite of variables to explore the environmental effects on canopy structure recovery.

(1) Climate: nineteen bioclimatic variables from the WorldClim 2.1 database (1 km resolution), representing long-term temperature (including bio_1 to bio_11 variables) and precipitation dynamics (including bio_12 to bio_19 variables). The bioclimatic variables represent annual trends (e.g., mean annual temperature and annual precipitation), seasonality (e.g., annual ranges of temperature and precipitation), and extreme or limiting environmental factors (e.g., temperatures in the coldest and warmest months and precipitation in the wet and dry quarters).

(2) Topography: the elevation, slope, and aspect were derived from the 1 km Shuttle Radar Topography Mission (SRTM) digital elevation model.

(3) Soil: soil properties at a 1 km resolution were obtained from the National Soil Information Grids of China, generated by Liu et al.[37] This dataset includes the following 17 soil variables at multiple depths across China: pH, soil organic carbon content, soil organic carbon density, total nitrogen content, total nitrogen density, total phosphorus content, total phosphorus density, total potassium content, total potassium density, cation exchange capacity, bulk density, coarse fragment content, soil sand content, soil silt content, clay content, soil texture classes, and thickness. For each soil property, we derived a representative value for the soil profile by calculating the mean (for continuous variables) or mode (for categorical variables) across all available vertical soil depth layers.

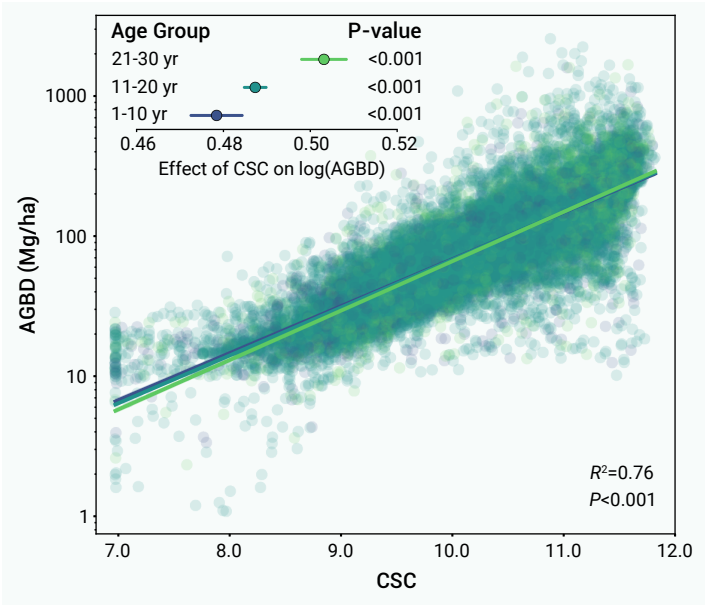

Figure 1. Influence of CSC on the AGBD across the three early recovery stages Lines represent the predictions from a linear mixed-effects model of log (AGBD), with shaded areas indicating 95% confidence intervals. Insets display the estimated coefficients (slopes) and their 95% confidence intervals for CSC within each stage.

(4) Forest Biome Classification: each recovery site was classified into one of 15 forest types using the updated vegetation map of China[38] and spatial nearest-neighbor assignment to analyze biome-specific dynamics. These forest types are cold-temperate and temperate mountain needleleaf forests; tropical monsoon rainforests; tropical rainforests; tropical needleleaf forests; temperate broadleaf deciduous forests; temperate mixed needleleaf and broadleaf deciduous forests; temperate needleleaf forests; subtropical and tropical bamboo forests and scrub; subtropical mixed broadleaf evergreen and deciduous forests; subtropical broadleaf evergreen forests; subtropical monsoon broadleaf evergreen forests; subtropical broadleaf deciduous forests; subtropical mountain coniferous, evergreen broadleaf and deciduous broadleaf mixed forests; subtropical broadleaf evergreen sclerophyllous forests; and subtropical needleleaf forests.

Given the disparate spatial resolutions of the data sources above, we performed a rigorous harmonization process. All the datasets were aggregated to a common 0.025° grid. Within each grid cell, we calculated the mean values for all the continuous variables and the modes for the categorical variables.

Defining early recovery phases

We delineated statistically significant, distinct phases within the early recovery time series by employing a data-driven approach to determine the optimal age intervals for grouping forest plots, thereby dividing the naturally regenerated forests restored within the 30-year focus period of this study into distinct recovery stages. The basic principles of this method are as follows: within each final age group, the simple linear relationship between CSC and AGBD is statistically significant ($P < 0.05$). We use this standard to ensure that each defined recovery stage has a sufficiently strong and consistent structure–function signal to support subsequent, more complex modeling. Moreover, given that this study focuses primarily on natural forests restored in the first 30 years, we tested five age intervals: 1, 3, 5, 6, and 10 years, because they evenly divide 30 into distinct stages. Through testing, we determined that a 10-year interval is the first and narrowest width that meets these criteria. Based on this result, we established three stages for analysis,

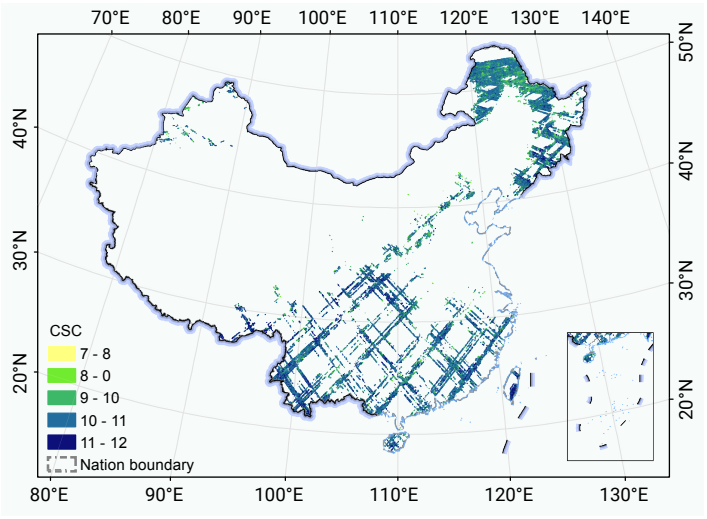

Figure 2. Distribution of CSC across China's natural forest recovery areas.

namely, 1–10 years, 11–20 years, and 21–30 years, corresponding to the early, middle, and late stages of natural forest restoration, respectively, within 30 years.

Modeling canopy structural complexity and aboveground biomass density

We investigated the varying intensities of CSC effects on AGBD across different recovery stages by using modeling approaches tailored to the data characteristics. Specifically, we employed a linear mixed-effects model (LMM) to model the natural logarithm of the AGBD. The logarithmic transformation was applied to meet the model's assumptions of normality of residuals and homoscedasticity. During the modeling process, the fixed effects of the model include CSC, three recovery stages, environmental factors, and crucially, the interaction term between CSC and recovery stages (CSC × Age), as shown in Eq. 1. The inclusion of this interaction term was strategic for verifyingtherobustnessofthestructure–functionrelationship.Byexplicitlytesting for significant temporal divergence in the scaling coefficients, we aim to distinguish dynamic ecological shifts in biomass allocation from static algorithmic artifacts.

To mitigate multicollinearity and reduce dimensionality among the environmental covariates, we applied principal component analysis (PCA) to the climate, terrain, and soil variable sets. For each dataset, we retained the first principal component (PC1), which accounted for 73.6%, 48.6%, and 33.6% of the variance in the original variables. Finally, all the continuous predictor variables (CSC and three PCs) were standardized (z-score transformation) to facilitate coefficient comparison and improve model convergence. Model performance was quantified using the conditional R^2 (Eq. 2), which assesses the variance explained by both fixed and random effects:

$$\begin{aligned}\ln(AGBD_{ij}) = (\beta_0 + b_j) + \beta_1 * CSC_{ij} + \beta_2 * Stage2 + \beta_3 * Stage3 \\ + \beta_4 * (CSC_{ij} * Stage2) + \beta_5 * (CSC_{ij} * Stage3) \\ + \beta_6 * PC1_{climate,ij} + \beta_7 * PC1_{topo,ij} + \beta_8 * PC1_{soil,ij} + \varepsilon_{ij}\end{aligned} \quad (1)$$

$$conditional\_R^2 = (\sigma_f^2 + \sigma_r^2)/(\sigma_f^2 + \sigma_r^2 + \sigma_\varepsilon^2) \quad (2)$$

where $\ln(AGBD_{ij})$ is the dependent variable, which represents the natural logarithm of the AGBD value for the i_{th} plot within the j_{th} spatial group. β_0 is the intercept, which represents the average $\ln(AGBD)$ for the reference age group Stage 1, when all the predictor variables are at their mean levels. b_j is the random intercept. $\beta_1,\ldots,\beta_8$ are the fixed effect coefficients. Stage2 and Stage3 represent the age groups. $PC1_{climate\_ij}, PC1_{topo\_ij}, PC1_{soil\_ij}$ are the first principal components of the climate, topography, and soil variable sets after PCA. ε_{ij} is a residual, representing random error not explained by the model. σ_f^2 is the variance explained by fixed effects, σ_r^2 is the variance explained by random effects, and σ_ε^2 is the residual variance.

Analyzing biome-level structural differences during restoration

We quantified the trajectory of CSC changes with age and explored the growth characteristics and differences in CSC across forest biomes by calculating the annual average CSC and its 95% confidence intervals at the national scale and for each forest biome. Using these results, we conducted a simple linear regression analysis to explore trends in the CSC across different forest biomes with age. We subsequently quantified pairwise differences in mean CSC across all 15 forest biomes within the three defined early recovery stages using the methods described below to analyze differences in CSC recovery trajectories across biomes. First, we used one-way Welch's ANOVA to test for overall differences in mean CSC across all forest biomes. We opted for Welch's ANOVA over the standard ANOVA because it is more robust to violations of the homogeneity of variance assumption (heteroscedasticity). These conditions were confirmed by Levene's test. After obtaining statistically significant results from Welch's ANOVA, we conducted pairwise comparisons using the Games–Howell post hoc test to identify which specific forest biomes differed significantly. The Games–Howell test is the most direct and appropriate follow-up analysis for Welch's ANOVA, as it does not assume homogeneity of variances and provides reliable p-values even under heteroscedasticity. All tests were performed at the $P < 0.05$ significance level.

Identifying dynamic environmental drivers

We developed a dynamic attribution framework to identify the environmental drivers of the differences in CSC across forest biomes during recovery. To ensure robust attribution and mitigate multicollinearity among predictors, we implemented a stratified feature selection strategy. First, we classified candidate environmental factors into four functional categories: temperature, precipitation, soil, and terrain. Within each category, we employed a stepwise forward selection procedure combining Mutual Information (MI) and Pearson correlation. We calculated the MI between the CSC and each variable to capture potential nonlinear relationships. Variables were ranked by MI score in descending order. The top-ranked variable was selected first, and subsequent variables were iteratively added to the subset only if their pairwise Pearson correlation coefficient with any already selected variable in that group was below a threshold of 0.8. This process was repeated until the top three independent predictors were retained for each category, constructing a concise and informative 12-variable feature set for each biome.

Using these features, we trained an eXtreme Gradient Boosting (XGBoost) model for each restoration stage of each forest biome to predict the CSC. Model predictive performance was evaluated using R^2 and Root Mean Square Error (RMSE) to ensure reliability, with the data split into 80% for training and 20% for validation. We subsequently employed the Shapley Additive exPlanations (SHAP) method to interpret these predictive models. SHAP offers a game-theoretic approach that assigns model predictions to each input feature. We used the mean absolute SHAP value for each feature as its global importance score, then summed the SHAP values of the features in each category to calculate that category's overall importance. We also identified the most significant influencing features for each forest biome at each stage and quantified the direction of their effects. Finally, we conducted Monte Carlo simulations to assess the robustness of the obtained driver importance over time. Specifically, for each forest biome at each stage, the entire process (data partitioning, model training, and SHAP attribution) was repeated 50 times. This process generated a series of importance score distributions for each driver, allowing us to calculate the mean and 95% confidence interval, thereby providing a statistically robust assessment of how forest age influences the control of environmental factors over CSC. The geopandas, pandas, statsmodels, pingouin, scikit-learn, xgboost, and shap libraries in Python 3.9 were used in these analyses.

RESULTS

Canopy structure–biomass relationships are strengthened during early forest recovery

We first observed the dynamic evolution of the relationship between canopy structure and function using the restored natural forest distribution and age data collected in China over the past 30 years (Figure 1). The linear mixed-effects model constructed for the AGBD and CSC indicates that CSC is

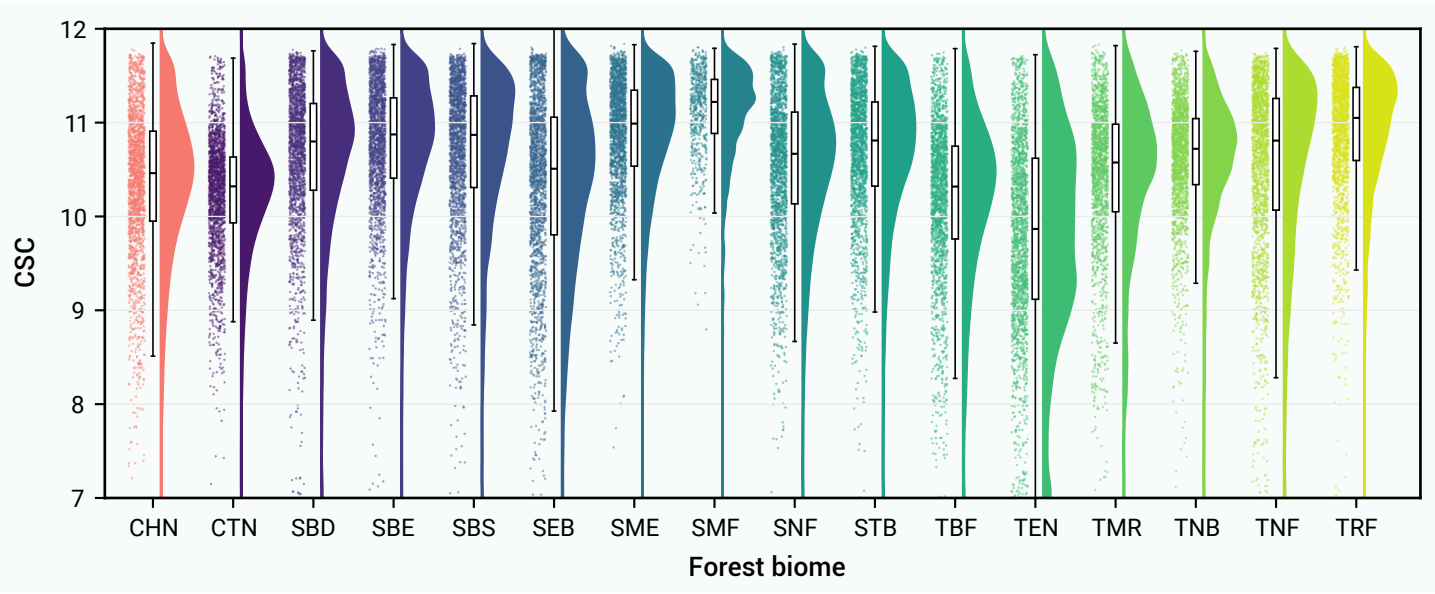

Figure 3. Distributions of CSC values across various forest biomes CHN: the whole recovered natural forests; CTN, cold-temperate and temperate mountain needleleaf forest; SBD, subtropical broadleaf deciduous forest; SBE, subtropical broadleaf evergreen forest; SBS, subtropical broadleaf evergreen sclerophyllous forest; SEB, subtropical mixed broadleaf evergreen and deciduous forest; SME, subtropical monsoon broadleaf evergreen forest; SMF, subtropical mountain coniferous, evergreen broadleaf and deciduous broadleaf mixed forest; SNF, subtropical needleleaf forest; STBs subtropical and tropical bamboo forest and scrub; TBF, temperate broadleaf deciduous forest; TEN, temperate needleleaf forest; TMR, tropical monsoon rainforest; TNB, temperate mixed needleleaf and broadleaf deciduous forest; TNF, tropical needleleaf forest; TRF, tropical rainforest.

one of the primary determinants of the AGBD throughout the entire 30-year period of forest restoration, as evidenced by the high explanatory power of the model (R^2 = 0.76) (Figure 1). These findings underscore the fundamental role of the canopy structure in biomass accumulation during the early stages of restoration.

Crucially, however, this structure-function coupling was not static. The interaction term between CSC and forest age was highly significant (P < 0.001), indicating that the strength of the relationship intensifies as forests mature (Figure 1). In the first stage of this study, the AGBD significantly increased with increasing CSC (P < 0.001), with an enhancement intensity of 0.48 (Figure 1). In subsequent stages, this positive effect significantly strengthened, with the enhancement intensity increasing to 0.51 (Figure 1). This progressive steepening of the positive effect indicates that the influence of canopy structure on biomass storage is not a fixed constant but gradually increases with age, reflecting a shift towards structure-dependent biomass accumulation in mature forests.

Natural restoration of the forest CSC follows distinct biogeographical patterns

After understanding this dynamic relationship between structure and function, we investigated how it manifests across different forest biomes, using the CSC as the primary indicator to quantify canopy-structure recovery trajectories. As shown in Figures 2-4, the recovery of CSC in China's natural forests follows distinct biogeographic patterns, leading to differences in recovery pathways across forest biomes.

The distribution pattern of the CSC in China's restored natural forests over the past three decades has exhibited distinct latitudinal and climatic gradients (Figure 2). The regions with the highest CSC are predominantly located in humid tropical and subtropical areas, where the average CSC exceeds 10 (Figure 2). In contrast, as latitude increases, the CSC of China's restored natural forests decreases, and the CSC in temperate and cold temperate zones is generally lower (Figure 2). Quantifying the distribution of the CSC across different forest biomes more explicitly demonstrates the structural heterogeneity of these restored natural forests (Figure 3). For example, tropical rainforests, tropical monsoon rainforests, and subtropical broadleaf evergreen forests presented the highest median CSC values (Figure 3). Conversely, the median CSC values and the distribution of values were lower for the cold–temperate and temperate mountain needleleaf forests (Figure 3).

We also quantified the developmental trajectories of the CSC in each biome over these 30 years, which indicated three distinct CSC recovery patterns (Figure 4). The first is an extremely significant increasing trend (P < 0.001) that occurs in most forest biomes, especially in subtropical forests, where it is particularly pronounced (Figure 4). Examples include subtropical needleleaf forest (R^2 = 0.89, P < 0.001) (Figure 4I), subtropical broadleaf evergreen forest (R^2 = 0.88, P < 0.001) (Figure 4D), and subtropical monsoon broadleaf evergreen forest (R^2 = 0.87, P < 0.001) (Figure 4G). The second shows a significant increasing pattern, with relatively moderate increases in two forest types: subtropical and tropical bamboo forestland and scrub (R^2 = 0.22, P < 0.01) and temperate needleleaf forest (R^2 = 0.25, P < 0.01) (Figures 4J & O). The third type is the nonsignificant development pattern, which primarily occurs in cold–temperate and temperate Mountain needleleaf forest (R^2 = 0.05, ns) and subtropical mountain coniferous, evergreen broadleaf and deciduous broadleaf mixed forest (R^2 = 0.06, ns) (Figures 4B & H). These two types of CSC have exhibited complex, nonlinear trajectories over the past three decades, with no significant increasing trend.

We compared the CSC values of different forest biomes at various stages of recovery and calculated their average values and the differences between them, as shown in Figure 4. The results indicate that differences in CSC values among most forest biomes were already present in the initial recovery stage (Figure 5). As time progressed, these differences generally showed a trend toward increasing divergence (Figure 5). These findings suggest that biogeographic factors largely determine the developmental trajectory of the CSC in these forest biomes. Specifically, during the first recovery stage, compared with other subtropical and temperate forests, forest biomes in tropical regions, such as tropical rainforests and tropical monsoon rainforests, presented higher CSC values (Figure 5A). In contrast, forest communities in subtropical, temperate, and cold–temperate zones, such as subtropical mountain coniferous, evergreen broadleaf and deciduous broadleaf mixed forest, and cold–temperate and temperate mountain needleleaf forest, presented relatively low CSC values in the initial stage (Figure 5A). Moreover, this difference was statistically significant (P < 0.05) across most forest biomes during the initial phase (Figure 5A). By the second and third phases, these significant differences persisted and tended to gradually widen, although they were not very pronounced (Figures 5B-C).

Shifting environmental signatures define the trajectory of forest CSC recovery

The significant differences in CSC across forest types at various stages of restoration prompted us to further identify the environmental drivers underlying these variations. Prior to interpreting these drivers, we evaluated the

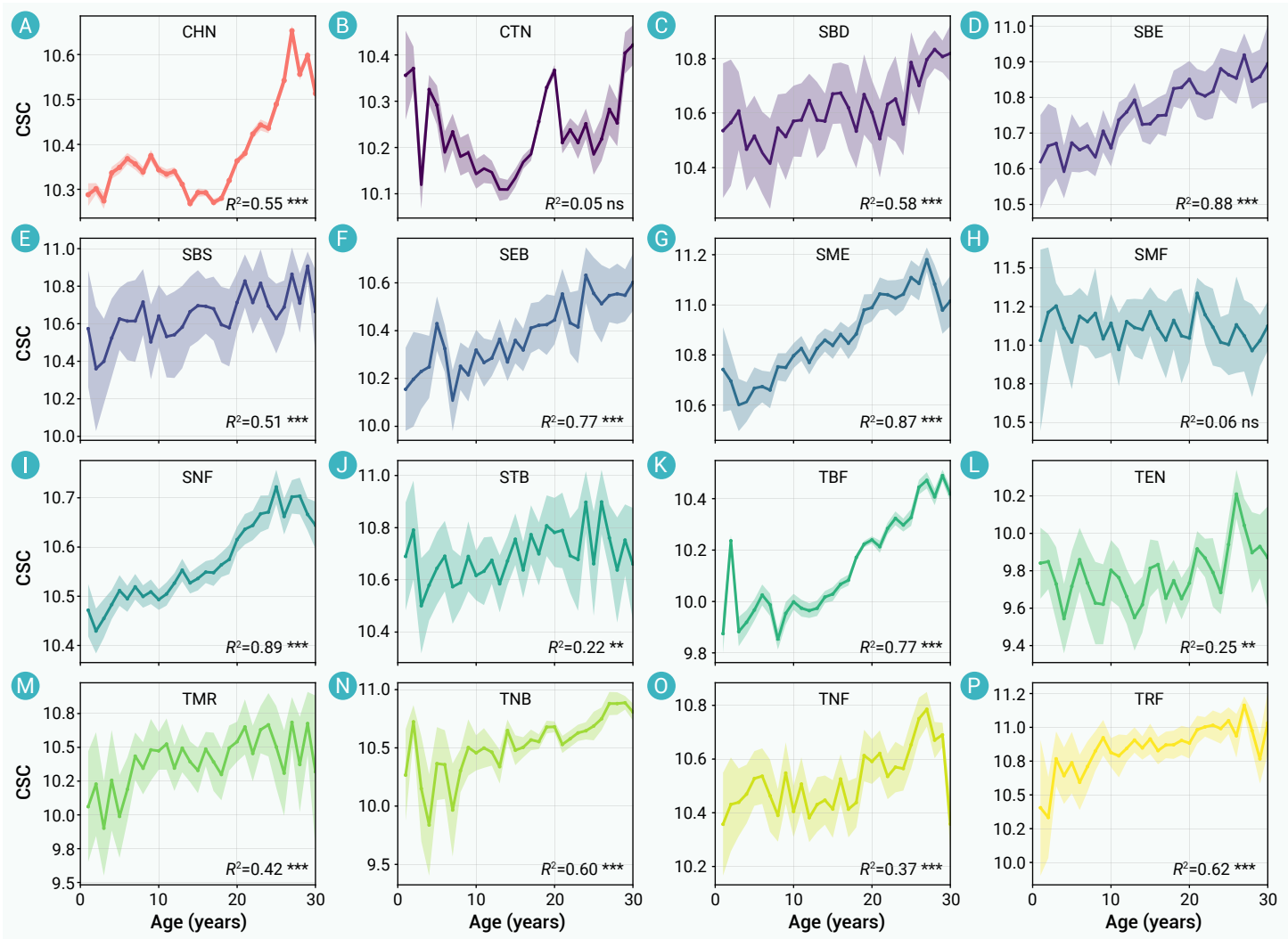

Figure 4. Temporal trajectories of CSC values over a 30-year period for all forests combined and for each forest type across China (A–P) represent all the restored natural forests in China (CHN) during the past 30 years; cold–temperate and temperate mountain needleleaf forests; subtropical broadleaf deciduous forests; subtropical broadleaf evergreen forests; subtropical broadleaf evergreen sclerophyllous forests; subtropical mixed broadleaf evergreen and deciduous forests; subtropical monsoon broadleaf evergreen forests; subtropical mountain coniferous, evergreen broadleaf and deciduous broadleaf mixed forests; subtropical needleleaf forests; subtropical and tropical bamboo forest and scrub; temperate broadleaf deciduous forests; temperate needleleaf forests; tropical monsoon rainforests; temperate mixed needleleaf and broadleaf deciduous forests; tropical needleleaf forests; and tropical rainforests. The analysis suggested that while most forest types exhibit a significant increase in structural complexity with age, the rate and statistical significance of this development vary substantially. Lines in figures represent the mean trend from linear regression, with shaded areas indicating 95% confidence intervals. R^2 values and significance levels are provided for each regression line (ns: not significant; *: $P < 0.05$; **: $P < 0.01$; ***: $P < 0.001$).

predictive reliability of our biome-specific XGBoost models. The models exhibited robust performance across all datasets, with a mean R^2 of 0.54 (peaking at 0.78) and RMSE ranging from 0.20 to 0.59 (Table S1). While predictive power varied across biomes due to inherent environmental heterogeneity, most models effectively captured the dominant gradients. Based on this robust modeling framework, the SHAP analysis indicates that the influence of environmental factors varies dynamically across restoration stages and differs markedly among forest biomes (Figures 6-7).

Specifically, in the first phase, at the national scale, temperature was the most important factor influencing CSC, with the temperature annual range being the most significant indicator among the temperature variables and exerting a negative effect (Figures 6 & 7A, S2-S3). Thus, lower temperature ranges (i.e., more thermally stable climates) are associated with higher CSC values across nearly all forest types. Soil was the second most influential factor, followed by topography and precipitation (Figure 6). In terms of forest biomes, in addition to precipitation, other factors exhibited the greatest influence across different forest types (Figure 6). Among them, temperature was the most critical factor affecting CSC development in five forest biomes: subtropical broadleaf deciduous forest; subtropical broadleaf evergreen sclerophyllous forest; subtropical mountain coniferous, evergreen broadleaf and deciduous broadleaf mixed forest; Subtropical needleleaf forest; and subtropical and tropical bamboo forest and scrub (Figures 6C, E, H-J & S2). For these five biomes, the most influential individual indicators were temperature seasonality, mean diurnal range, annual precipitation, and slope (Figures 7A & S3). Topography was the primary factor influencing CSC changes in the tropical monsoon rain forest during this stage (Figure 6M), with elevation being the most significant indicator of the CSC variation in the tropical monsoon rainforest (Figures 7A & S2-S3). Soil was the primary factor influencing CSC development in nine forest biomes: cold–temperate and temperate mountain needleleaf forests; subtropical broadleaf evergreen forests; subtropical mixed broadleaf evergreen and deciduous forests; subtropical monsoon broadleaf evergreen forests; temperate broadleaf deciduous forests; temperate needleleaf forests; temperate mixed needleleaf forests; tropical needleleaf forests; and tropical rainforests (Figures 6B, D, F-G, K-L, N-P & S2). The key indicators affecting these biomes were soil thickness, bulk density, precipitation seasonality, coarse fragment content, soil thickness, soil organic carbon, total phosphorus density, minimum temperature in the coldest month, and cation exchange capacity (Figures 7A & S3). Overall, temperature and soil were the dominant factors influencing CSC development in the early stages of the restoration of natural forests in China.

As forests enter the second stage of restoration, the overall influence of environmental factors tends to decrease across the entire forest ecosystem

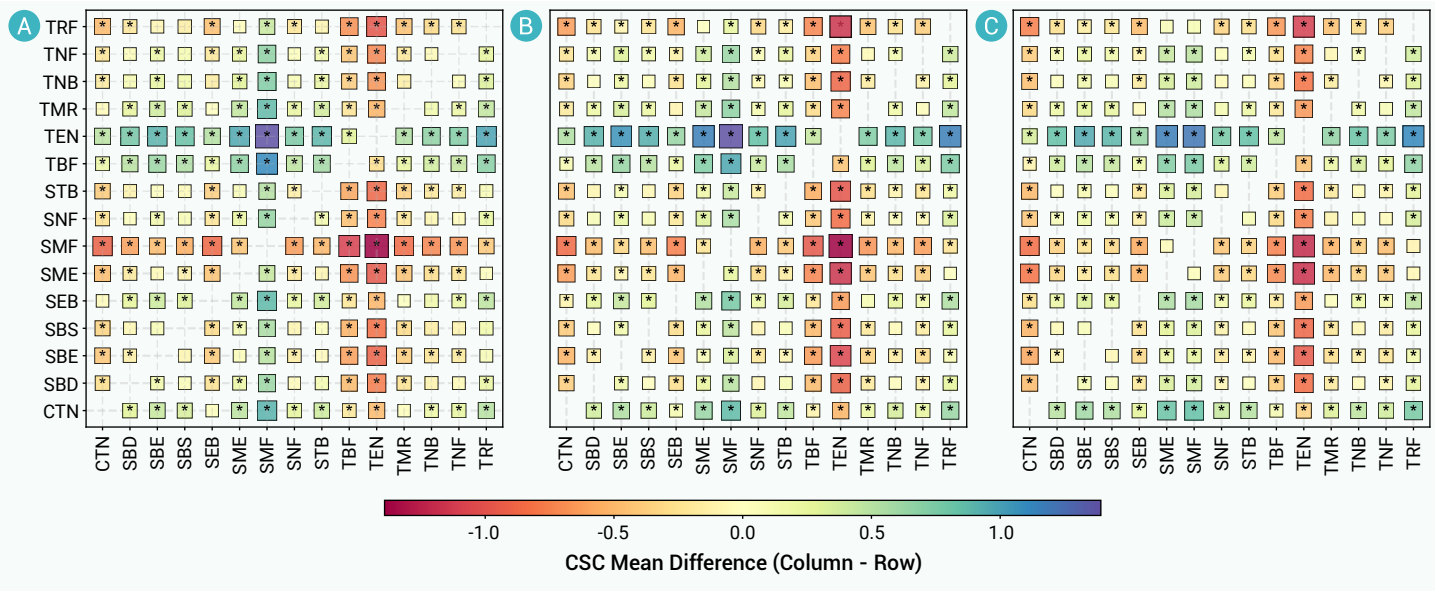

Figure 5. Persistent structural hierarchy among forest biomes during early recovery Pairwise comparisons of mean CSC values among 15 distinct forest biomes across three sequential early recovery stages: 1–10 years (A), 11–20 years (B), and 21–30 years (C). Each cell represents the mean difference in the CSC value, which was calculated as the value for the forest biome on the x-axis (column) minus the value for the forest biome on the y-axis (row). Consequently, warmer colors (yellow) indicate that the y-axis (row) forest biome has a higher CSC. In comparison, cooler colors (purple) indicate that the x-axis (column) forest biome has a higher CSC. * Within a cell, the difference is statistically significant ($P < 0.05$).

and all forest biomes (Figure 5). The sequence of the influence of different factors on the CSC and the primary impact indicators in various forest biomes also changed (Figures 6 & 7B). During this stage, temperature became the most significant factor in only the CSC development of subtropical broadleaf deciduous forest and temperate mixed needleleaf and broadleaf deciduous forest, with the leading indicators for these two types remaining the same as those in the first stage (Figures 6C, N & S4-S5). Precipitation still did not show a prominent overall effect on any of the biomes (Figure 6). Compared with those in the first stage, topographic factors became the dominant factors influencing CSC in more forest types, including subtropical and tropical bamboo forest and scrub, tropical monsoon rainforest, and tropical rainforest (Figures 6J, M & P); however, elevation was the only topographic factor that emerged as the most critical indicator for CSC in the above tropical monsoon rainforest, whereas temperature seasonality and annual precipitation were the primary indicators for subtropical and tropical bamboo forest and scrub and tropical rainforest (Figures 7B & S4-S5). Soil factors continued to stand out during this stage, not only replacing temperature as the most critical factor in the CSC recovery of China's forests in general but also becoming the dominant factor in the CSC changes in 10 forest biomes: cold–temperate and temperate mountain needleleaf forest; subtropical broadleaf evergreen forest; subtropical broadleaf evergreen sclerophyllous forest; subtropical mixed broadleaf evergreen and deciduous forest; subtropical monsoon broadleaf evergreen forest; subtropical mountain coniferous, evergreen broadleaf and deciduous broadleaf mixed forest; subtropical needleleaf forest; temperate broadleaf deciduous forest; temperate needleleaf forest; and tropical needleleaf forest (Figures 6B, D-I, K-L, O & S4). The primary indicators influencing CSC changes in these 10 biomes were soil thickness, bulk density, soil organic carbon density, slope, soil thickness, soil sand content, mean temperature in the warmest quarter, soil thickness, soil organic carbon, and minimum temperature in the coldest month, respectively (Figures 7B & S5). Hence, during this period, soil factors undeniably became the most dominant factors influencing changes in CSC during the natural forest restoration process.

In the third stage, the overall influence of environmental factors increased again. The dominant factor categories and key indicators changed once more compared with the previous two stages (Figure 6). Precipitation became the most critical factor affecting the recovery of natural forest CSC nationwide, with annual precipitation emerging as the most significant indicator (Figures 6A & S6-S7). Similarly, precipitation played the most important role in the CSC recovery of subtropical needleleaf forests, with precipitation during the driest month being the most influential indicator (Figures 6I, C & S6-S7). Temperature-related factors also began to dominate the CSC changes in more forest biomes, including cold–temperate and temperate mountain needleleaf forests; subtropical broadleaf evergreen sclerophyllous forests; subtropical mountain coniferous, evergreen broadleaf and deciduous broadleaf mixed forests; temperate mixed needleleaf and broadleaf deciduous forests; tropical needleleaf forests; and tropical rainforests (Figures 6B, E, H, N-P & S6). The key indicators for these types were all related to temperature, including the mean diurnal range, minimum temperature in the coldest month, annual temperature range, and mean temperature in the coldest quarter (Figures 7C & S7). The role of topographic factors diminished, showing a significantly greater impact only on the CSC development of the tropical monsoon rain forest, where elevation was the most critical indicator influencing CSC changes in this type (Figures 6M, 7C & S6-S7). The influence of soil factors also weakened to some extent and played a dominant role in the CSC development of the subtropical broadleaf deciduous forest, subtropical broadleaf evergreen forest, subtropical mixed broadleaf evergreen and deciduous forest, subtropical monsoon broadleaf evergreen forest, temperate broadleaf deciduous forest, and temperate needleleaf forest (Figures 6C-D, F-G, K-L & S6). The most influential indicators for these biomes were soil silt content, temperature seasonality, coarse fragment content, soil thickness, annual precipitation, and soil organic carbon content (Figures 7C & S7). At this stage, the impacts of soil and topographic factors on subtropical and tropical bamboo forest and scrub were similar and significantly greater than those of temperature and precipitation factors (Figures 6J & S6-S7). In summary, during the third stage of recovery, the role of precipitation factors increased notably compared with the previous two stages. At the same time, temperature and soil remained the two most critical factors.

DISCUSSION

Many studies have explored the relationships between the structure and ecological functions of large-scale forest restoration.[39-41] However, a significant portion of studies rely on generalized, static assumptions, often treating the scaling relationship between structure and function as a fixed constant to ensure tractability.[42-44] To challenge this paradigm, we integrated time-series data to propose a dynamic, stage-dependent framework for understanding the regeneration process. Our key finding is that during the early phase of natural forest restoration (the first 30 years in this study), the positive coupling between CSC and AGBD is not static but strengthens significantly with stand age (Figure 1). Moreover, distinct structural fingerprints for each

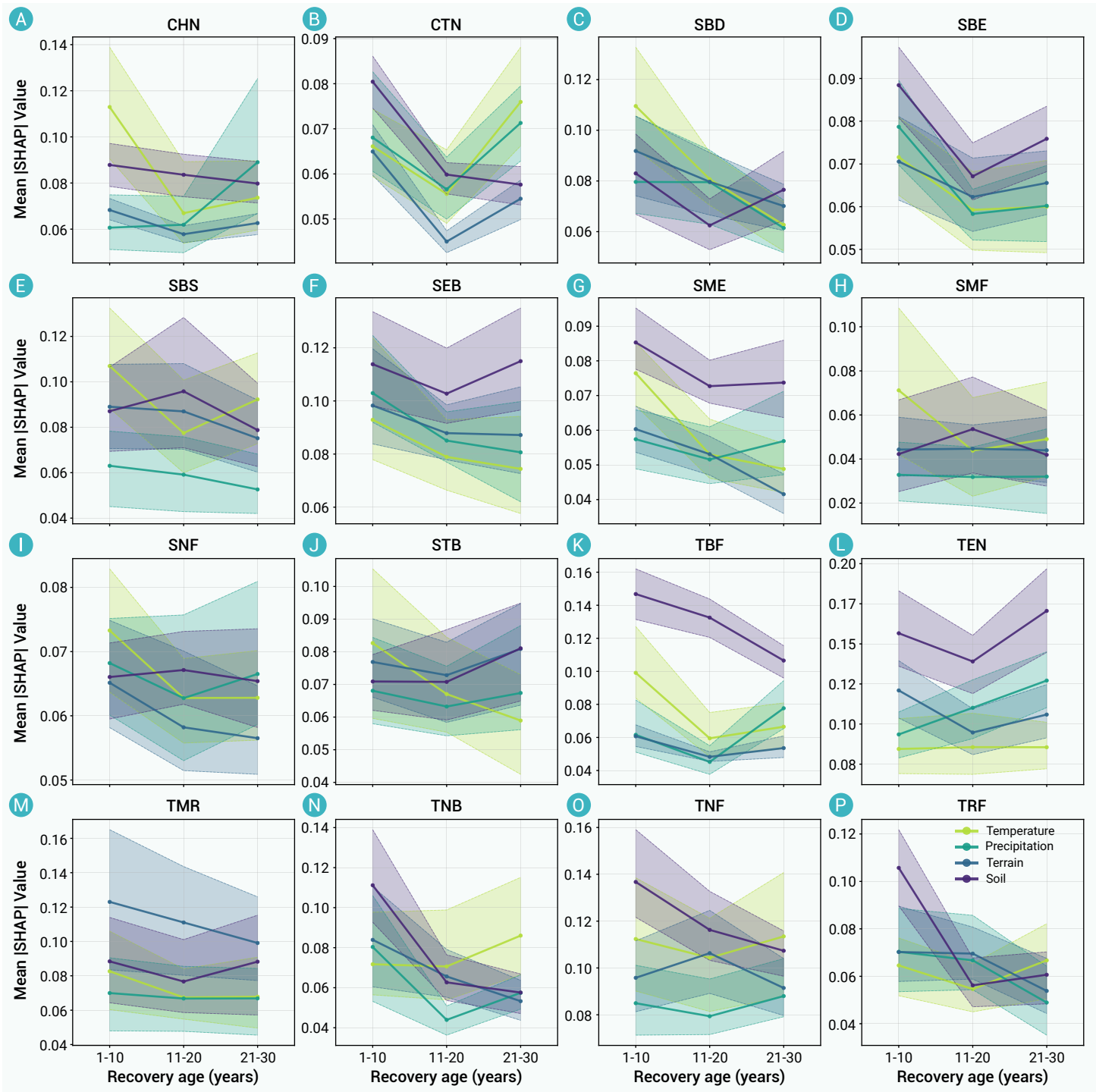

Figure 6. The shifting relative importance of four major environmental driver categories (temperature, precipitation, terrain, and soil) on CSC Importance is quantified by the mean absolute SHAP value across three recovery stages for all of China's forests and 15 distinct forest biomes. (A–P) represent all the restored natural forests in China (CHN) during the past 30 years: cold–temperate and temperate mountain needleleaf forests; subtropical broadleaf deciduous forests; subtropical broadleaf evergreen forests; subtropical broadleaf evergreen sclerophyllous forests; subtropical mixed broadleaf evergreen and deciduous forests; subtropical monsoon evergreen forests; subtropical mountain coniferous, evergreen broadleaf and deciduous broadleaf mixed forests; subtropical needleleaf forests; subtropical, tropical bamboo forest and scrub; temperate broadleaf deciduous forests; temperate needleleaf forests; tropical monsoon rainforests; temperate mixed needleleaf and broadleaf deciduous forests; tropical needleleaf forests; and tropical rainforests.

forest biome form early and persist throughout recovery, driven by a series of predictable environmental constraints that evolve over time (Figures 2-5).

Dynamic changes in the functional role of the canopy structure constitute a core aspect of this study. The increasingly strengthened positive relationship between CSC and AGBD signifies a fundamental shift in biomass allocation strategies—from horizontal resource competition to vertical resource optimization. In young forests with sparse canopies, trees prioritize rapid vertical growth and horizontal crown expansion to occupy space, a strategy driven by fast life-history traits that prioritize colonization speed over structural efficiency.[45-48] As competition intensifies and the canopy closes, it creates heterogeneous microenvironments that allow species with differing functional traits (e.g., shade tolerance vs. light demand) to coexist vertically, thereby maximizing light interception and total carbon storage per unit volume.[49,50] Crucially, this observed temporal shift—from a lower to a higher scaling coefficient—provides strong ecological evidence that the temporal dynamics of the CSC–AGBD relationship are driven by evolving biological

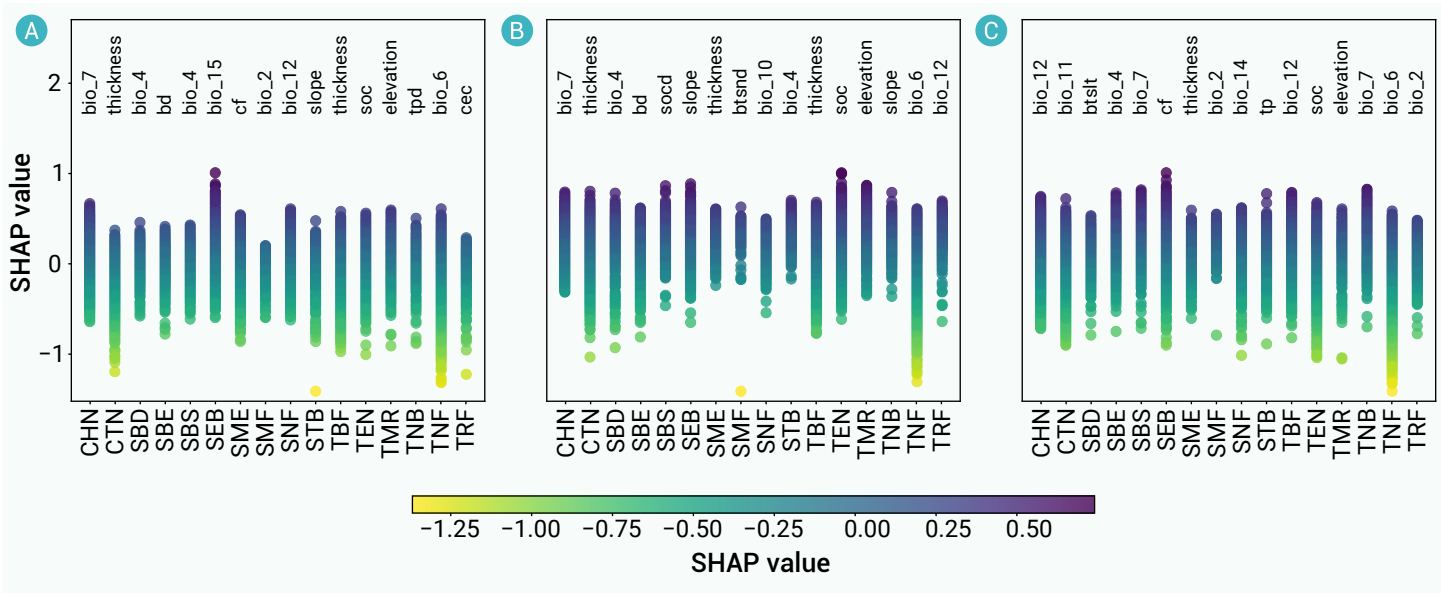

Figure 7. Detailed SHAP summary plots for the most influential individual variables within each recovery stage, ranked by their global mean importance (A) The first recovery stage. (B) The second recovery stage. (C) The third recovery stage. Each point represents the SHAP value for a single observation, illustrating both the magnitude and direction of the effect of a variable on the CSC prediction. The variables included bio_2, bio_4, bio_6, bio_7, bio_10, bio_11, bio_12, bio_14, bio_15, bd, btslt, btsnd, cec, cf, soc, socd, tp, and tpd, which are the mean diurnal range, temperature seasonality, minimum temperature in the coldest month, annual temperature range, mean temperature in the warmest quarter, mean temperature in the coldest quarter, annual precipitation, precipitation in the driest month, precipitation seasonality, bulk density, soil silt content, soil sand content, cation exchange capacity, coarse fragment content, soil organic carbon content, soil organic carbon density, total phosphorus content, and total phosphorus density.

mechanisms, even though the absolute magnitude of the baseline correlation may be influenced by data provenance.

Differences in structural trajectories across forest biomes and their persistence (Figures 2-5) are driven by a predictable, phase-dependent environmental control mechanism (Figure 6). In the initial stage of forest restoration, forest establishment is influenced by a strong dual environmental filter. Macroclimate determines the potential species pool, while microsite conditions dictate colonization success. Consistent with Condit et al,[51] temperature—particularly the annual temperature range—dominates at the national scale.[52] A lower annual temperature range indicates a milder, more predictable environment, which significantly reduces extreme temperature stress on seedlings and young trees, thereby improving survival rates and early growth efficiency.[53] Concurrently, local soil conditions (e.g., thickness and bulk density) and topographic factors (which govern local hydrothermal gradients) serve as the second filter.[54-58] In particular, in boreal, temperate, and some nutrient-limited tropical forests, superior soil conditions provide seedlings with an initial advantage.[54-56]

As forests entered the second phase of recovery, the primary driver of CSC shifted from macroclimate to soil properties, accompanied by a decrease in the overall explanatory power of environmental factors (Figure 6). This shift results from microclimatic buffering and intensified belowground competition. Canopy closure shields the understory from macro-temperature fluctuations, reducing the direct impact of climate.[59] Conversely, increasing stand density intensifies competition for limiting belowground resources.[60] Soil heterogeneity exerts an amplified effect during this stage: patches with superior edaphic conditions (e.g., higher organic carbon or favorable texture) facilitate faster growth and canopy dominance, whereas resource-poor patches inhibit growth.[61-65] This soil-mediated growth differentiation creates vertical stratification and horizontal heterogeneity, driving the increase in CSC.[66] The decline in the overall influence of environmental factors may suggest that as biomass accumulates, biological interactions within the biome (such as competition and allelopathy) become increasingly significant, leading to a degree of "decoupling" of system dynamics from direct control by the external environment.

Upon entering the final stage of our study, the pattern of driving factors was restructured again, with the combined influence of environmental factors regaining strength (Figure 6). Precipitation became the primary driver on a national scale for the first time. In contrast, temperature regained dominance in more forest types (Figures 6-7). Mature stands with high leaf area indices sustain massive transpiration demands; thus, regional water supply (annual precipitation) sets the upper limit for biomass capacity and productivity.[67-71] Meanwhile, temperature regains importance as a regulator of metabolic rates and phenology (e.g., growing season length and dormancy), rather than as a mere survival filter.[72-76] Ultimately, the interaction of water availability and thermal energy maintains the dynamic equilibrium of these complex ecosystems.[77-79] In summary, our findings not only deepen the theoretical understanding of ecological restoration but also have significant practical implications. Forest restoration strategies must be dynamic and phased: prioritizing climate matching and microsite selection during establishment; managing density and soil resources to facilitate structural differentiation in mid-term phases; and accounting for regional water carrying capacity and phenological shifts under climate change for long-term sustainability.

We must acknowledge that the methods and data used in this study have certain limitations, which also point to the way for future research. First, we adopted the space-for-time substitution method, which assumes that spatial gradients can reliably represent temporal changes. Nevertheless, this assumption is challenged under conditions of rapid, nonstationary environmental change.[34] Second, forests that began to recover during different historical periods faced varying climatic conditions, which may have altered their developmental trajectories, and our time series may not fully capture these changes.[80,81] Third, although remote sensing observations provide unprecedented spatial coverage, their application at this scale also presents validation challenges, as we currently lack long-term ground monitoring data.[43,82] Fourth, regarding the correlation between CSC and AGBD, we must explicitly acknowledge the potential concern of methodological dependence (i.e., circularity issue), as both metrics in our primary analysis derive from GEDI observations. To rigorously test this, we conducted a sensitivity analysis using an independent national-scale AGB product, which is produced from ground-survey data combined with spectral features, topographic data, climate data, and soil properties, without directly using GEDI data.[83] This independent validation confirmed that the positive direction of the CSC–AGBD coupling and its temporal strengthening pattern are robust and reproducible (Figure S8). However, it is crucial to note that the absolute explanatory power (R^2) declined to 0.20 when using the independent dataset. This large reduction indicates that the absolute strength of the structure–function coupling is highly sensitive to the choice of biomass products and should be interpreted with caution. We carefully reflect on this substantial decline and attribute it to two main factors. First, the extremely

high correlation observed in our original analysis was partially inflated by methodological covariance, as both CSC and GEDI-based AGBD inherently share overlapping structural information (e.g., lidar-derived canopy height metrics). Second, the independent AGBD product relies on different model architectures, integrates multi-source data (e.g., optical, soil, terrain, and climate variables), and employs spatial aggregation and smoothing algorithms. These processes tend to dampen the fine-scale, localized structural heterogeneity that CSC captures, thereby naturally reducing the covariance. Therefore, while our study confidently highlights the robust temporal dynamics of their interaction, the absolute magnitude of the coupling reported originally partly reflects shared data provenance. Fifth, we acknowledge the inherent uncertainties associated with GEDI data in topographically complex regions. As a large-footprint lidar system, GEDI waveforms are susceptible to pulse broadening on steep slopes, which can mix ground and canopy signals and artificially inflate structural metrics.[84] In our data processing, we applied rigorous waveform-level quality controls (requiring sensitivity > 0.9, l2_quality_flag = 1, and degrade_flag = 0) to exclude severely degraded signals and mitigate these artifacts. However, because a direct topographic slope mask was not applied, residual terrain-induced biases may still exist, particularly in mountainous biomes (e.g., Southwest China). Crucially, while this may inflate the absolute magnitude of CSC in some areas, it does not undermine our core findings. Topography is strictly static over our 30-year study period; thus, a static topographic bias cannot generate the dynamic, age-dependent strengthening of the structure–biomass coupling observed in this study. The temporal trajectories reported here, therefore, reflect genuine biological stand development. Nonetheless, future studies utilizing high-resolution small-footprint airborne lidar are needed to perfectly disentangle fine-scale topography from complex canopy structures.

Future research should consider integrating our findings with long-term forest inventory networks and process-based ecological models to mechanistically validate the observed structure–function dynamics and the inferred drivers.[85] Finally, our 30-year time series study indicated critical early stages in the natural forest restoration process, but understanding the dynamic mechanisms of the transition to an old-growth forest status still requires integration with long-term monitoring data.[86] Nevertheless, our research suggests that the structural fingerprint of a recovering forest is not a static image but an evolving signature written by a dynamic interplay between age and the environment. Decoding this ecological signature is fundamental to accurately predicting the fate of Earth's forests, improving the efficacy of our restoration efforts, and successfully navigating the challenges of stewardship in the Anthropocene.

CONCLUSION

In conclusion, our comprehensive analysis of natural forest recovery in China moves beyond static assessments to present a dynamic, stage-dependent process. We found that the structural fingerprint of a recovering forest is not a fixed attribute but an evolving signature shaped by a predictable interplay between stand age and shifting environmental drivers. The recovery trajectory is initially limited by temperature filters, then becomes constrained by soil-mediated resource competition as canopies close, and ultimately is regulated by large-scale water availability. While we acknowledge the inherent uncertainties associated with space-for-time substitution and the observational nature of satellite-derived metrics, the robustness of these patterns across diverse biomes supports a compelling mechanistic framework. This dynamic perspective moves beyond "one-size-fits-all" restoration, offering a scientific basis for setting biome-specific, age-appropriate targets and for developing adaptive management strategies that can increase the success and resilience of global forest restoration efforts in the Anthropocene.

REFERENCES

1. Hua F., Bruijnzeel L. A., Meli P., et al. (2022). The biodiversity and ecosystem service contributions and trade-offs of forest restoration approaches. *Science* **376**:839–844. DOI:10.1126/science.abl4649
2. Williams B. A., Beyer H. L., Fagan M. E., et al. (2024). Global potential for natural regeneration in deforested tropical regions. *Nature* **636**:131–137. DOI:10.1038/s41586-024-08106-4
3. Chazdon R. and Brancalion P. (2019). Restoring forests as a means to many ends. *Science* **365**:24–25. DOI:10.1126/science.aax9539
4. Erbaugh J. T., Pradhan N., Adams J., et al. (2020). Global forest restoration and the importance of prioritizing local communities. *Nat. Ecol. Evol.* **4**:1472–1476. DOI:10.1038/s41559-020-01282-2
5. Robinson N., Drever C. R., Gibbs D. A., et al. (2025). Protect young secondary forests for optimum carbon removal. *Nat. Clim. Change* **15**:793–800. DOI:10.1038/s41558-025-02355-5
6. Camarretta N., Harrison P. A., Bailey T., et al. (2020). Monitoring forest structure to guide adaptive management of forest restoration: A review of remote sensing approaches. *New For.* **51**:573–596. DOI:10.1007/s11056-019-09754-5
7. Rodrigues R. R., Lima R. A. F., Gandolfi S., et al. (2009). On the restoration of high diversity forests: 30 years of experience in the Brazilian Atlantic Forest. *Biol. Conserv.* **142**:1242–1251. DOI:10.1016/j.biocon.2008.12.008
8. Chaves R. B., Durigan G., Brancalion P. H. S., et al. (2015). On the need of legal frameworks for assessing restoration projects success: New perspectives from São Paulo state (Brazil). *Restor. Ecol.* **23**:754–759. DOI:10.1111/rec.12267
9. Fu X., Zhang Z., Cao L., et al. (2021). Assessment of approaches for monitoring forest structure dynamics using bi-temporal digital aerial photogrammetry point clouds. *Remote Sens. Environ.* **255**:112300. DOI:10.1016/j.rse.2021.112300
10. Masek J. G., Hayes D. J., Joseph Hughes M., et al. (2015). The role of remote sensing in process-scaling studies of managed forest ecosystems. *For. Ecol. Manage.* **355**:109–123. DOI:10.1016/j.foreco.2015.05.032
11. Santoro G. B., Molin P. G., Viveiros J. M. S. M., et al. (2025). Monitoring the structure of restored forests and assessing aboveground carbon density through canopy metrics derived from digital aerial photogrammetry and LiDAR. *Restor. Ecol.* **33**:e70077. DOI:10.1111/rec.70077
12. Ruiz-Jaén M. C. and Aide T. M. (2005). Vegetation structure, species diversity, and ecosystem processes as measures of restoration success. *For. Ecol. Manage.* **218**:159–173. DOI:10.1016/j.foreco.2005.07.008
13. De Almeida D. R. A., Broadbent E. N., Ferreira M. P., et al. (2021). Monitoring restored tropical forest diversity and structure through UAV-borne hyperspectral and lidar fusion. *Remote Sens. Environ.* **264**:112582. DOI:10.1016/j.rse.2021.112582
14. Liu X., Ma Q., Wu X., et al. (2022). A novel entropy-based method to quantify forest canopy structural complexity from multiplatform lidar point clouds. *Remote Sens. Environ.* **282**:113280. DOI:10.1016/j.rse.2022.113280
15. Hu T., Liu X., Wu X., et al. (2025). Advance in forest canopy structural complexity research. *J Remote Sens-Prc.* **29**:83–101. DOI:10.11834/jrs.20244007
16. de Conto T., Armston J. and Dubayah R. (2024). Characterizing the structural complexity of the Earth's forests with spaceborne lidar. *Nat. Commun.* **15**:8116. DOI:10.1038/s41467-024-52468-2
17. Liu X., Feng Y., Hu T., et al. (2024). Enhancing ecosystem productivity and stability with increasing canopy structural complexity in global forests. *Sci. Adv.* **10**:eadl1947. DOI:10.1126/sciadv.adl1947
18. Fahey C., Choi D., Wang J., et al. (2025). Canopy complexity drives positive effects of tree diversity on productivity in two tree diversity experiments. *Ecology* **106**:e4500. DOI:10.1002/ecy.4500
19. LaRue E. A., Fahey R. T., Alveshere B. C., et al. (2023). A theoretical framework for the ecological role of three-dimensional structural diversity. *Front. Ecol. Environ.* **21**:4–13. DOI:10.1002/fee.2587
20. Gough C. M., Atkins J. W., Fahey R. T., et al. (2019). High rates of primary production in structurally complex forests. *Ecology* **100**:e02864. DOI:10.1002/ecy.2864
21. Chazdon R. L., Letcher S. G., van Breugel M., et al. (2006). Rates of change in tree communities of secondary neotropical forests following major disturbances. *Phil. Trans. R. Soc. B.* **362**:273–289. DOI:10.1098/rstb.2006.1990
22. Poorter L., Bongers F., Aide T. M., et al. (2016). Biomass resilience of Neotropical secondary forests. *Nature* **530**:211–214. DOI:10.1038/nature16512
23. Poorter H., Niklas K. J., Reich P. B., et al. (2012). Biomass allocation to leaves, stems and roots: meta-analyses of interspecific variation and environmental control. *New Phytol.* **193**:30–50. DOI:10.1111/j.1469-8137.2011.03952.x
24. Ehbrecht M., Seidel D., Annighöfer P., et al. (2021). Global patterns and climatic controls of forest structural complexity. *Nat. Commun.* **12**:519. DOI:10.1038/s41467-020-20767-z
25. Bazzaz F. A. (1990). The response of natural ecosystems to the rising global CO_2 levels. *Annu. Rev. Ecol. Evol. S.* **21**:167–196. DOI:10.1146/annurev.es.21.110190.001123
26. Cheng K., Zhang Y., Ren Y., et al. (2025). Natural forest restoration potential to mitigate climate change in China. *Earths Future* **13**:e2024EF005794. DOI:10.1029/2024EF005794
27. Bastin J.-F., Finegold Y., Garcia C., et al. (2019). The global tree restoration potential. *Science* **365**:76–79. DOI:10.1126/science.aax0848
28. Cheng K., Zhang Y., Yang H., et al. (2025). China's naturally regenerated forests currently have greater aboveground carbon accumulation rates than newly planted forests. *Commun. Earth Environ.* **6**:345. DOI:10.1038/s43247-025-02323-z
29. Nagy R. C., Rastetter E. B., Neill C., et al. (2017). Nutrient limitation in tropical secondary forests following different management practices. *Ecol. Appl.* **27**:734–755. DOI:10.1002/eap.1478
30. Phillips O. L., Aragão L. E. O. C., Lewis S. L., et al. (2009). Drought sensitivity of the amazon rainforest. *Science* **323**:1344–1347. DOI:10.1126/science.1164033
31. Stephenson N. L., Das A. J., Condit R., et al. (2014). Rate of tree carbon accumulation

increases continuously with tree size. *Nature* **507**:90–93. DOI:10.1038/nature12914
32. Chazdon R. L., Broadbent E. N., Rozendaal D. M. A., et al. (2016). Carbon sequestration potential of second-growth forest regeneration in the Latin American tropics. *Sci. Adv.* **2**:e1501639. DOI:10.1126/sciadv.1501639
33. Pugh T. A. M., Lindeskog M., Smith B., et al. (2019). Role of forest regrowth in global carbon sink dynamics. *Proc. Natl. Acad. Sci. USA* **116**:4382–4387. DOI:10.1073/pnas.1810512116
34. Evans M. E. K., Adler P. B., Angert A. L., et al. (2025). Reconsidering space-for-time substitution in climate change ecology. *Nat. Clim. Change* **15**:809–812. DOI:10.1038/s41558-025-02392-0
35. Duncanson L., Kellner J. R., Armston J., et al. (2022). Aboveground biomass density models for NASA's global ecosystem dynamics investigation (GEDI) lidar mission. *Remote Sens. Environ.* **270**:112845. DOI:10.1016/j.rse.2021.112845
36. Liang J., Gamarra J. G. P., Picard N., et al. (2022). Co-limitation towards lower latitudes shapes global forest diversity gradients. *Nat. Ecol. Evol.* **6**:1423–1437. DOI:10.1038/s41559-022-01831-x
37. Liu F., Wu H., Zhao Y., et al. (2022). Mapping high resolution national soil information grids of China. *Sci. Bull.* **67**:328–340. DOI:10.1016/j.scib.2021.10.013
38. Su Y., Guo Q., Hu T., et al. (2020). An updated vegetation map of China (1:1000000). *Sci. Bull.* **65**:1125–1136. DOI:10.1016/j.scib.2020.04.004
39. Chazdon and Lee R. (2014). Second growth: The promise of tropical forest regeneration in an age of deforestation. DOI:10.7208/chicago/9780226118109.001.0001
40. Griscom B. W., Adams J., Ellis P. W., et al. (2017). Natural climate solutions. *Proc. Natl. Acad. Sci. USA* **114**:11645–11650. DOI:10.1073/pnas.1710465114
41. Perea S. (2025). Listening to forest recovery. *Nat. Rev. Biodivers.* **1**:496–496. DOI:10.1038/s44358-025-00073-6
42. Saatchi S. S., Harris N. L., Brown S., et al. (2011). Benchmark map of forest carbon stocks in tropical regions across three continents. *Proc. Natl. Acad. Sci. USA* **108**:9899–9904. DOI:10.1073/pnas.1019576108
43. Avitabile V., Herold M., Heuvelink G. B. M., et al. (2016). An integrated pan-tropical biomass map using multiple reference datasets. *Global Change Biol.* **22**:1406–1420. DOI:10.1111/gcb.13139
44. McDowell N. G., Allen C. D., Anderson-Teixeira K., et al. (2020). Pervasive shifts in forest dynamics in a changing world. *Science* **368**:eaaz9463. DOI:10.1126/science.aaz9463
45. Binkley D., Stape J. L., Ryan M. G., et al. (2002). Age-related decline in forest ecosystem growth: An individual-tree, stand-structure hypothesis. *Ecosystems* **5**:58–67. DOI:10.1007/s10021-001-0055-7
46. Wright I. J., Reich P. B., Westoby M., et al. (2004). The worldwide leaf economics spectrum. *Nature* **428**:821–827. DOI:10.1038/nature02403
47. Kunstler G., Falster D., Coomes D. A., et al. (2016). Plant functional traits have globally consistent effects on competition. *Nature* **529**:204–207. DOI:10.1038/nature16476
48. Reich P. B. (2014). The world-wide 'fast–slow' plant economics spectrum: A traits manifesto. *J. Ecol.* **102**:275–301. DOI:10.1111/1365-2745.12211
49. Pretzsch H. (2014). Canopy space filling and tree crown morphology in mixed-species stands compared with monocultures. *For. Ecol. Manage.* **327**:251–264. DOI:10.1016/j.foreco.2014.04.027
50. Morin X. (2015). Species richness promotes canopy packing: A promising step towards a better understanding of the mechanisms driving the diversity effects on forest functioning. *Funct. Ecol.* **29**:993–994. DOI:10.1111/1365-2435.12473
51. Condit R., Engelbrecht B. M. J., Pino D., et al. (2013). Species distributions in response to individual soil nutrients and seasonal drought across a community of tropical trees. *Proc. Natl. Acad. Sci. USA* **110**:5064–5068. DOI:10.1073/pnas.1218042110
52. Seidl R., Thom D., Kautz M., et al. (2017). Forest disturbances under climate change. *Nat. Clim. Change* **7**:395–402. DOI:10.1038/nclimate3303
53. Hatfield J. L. and Prueger J. H. (2015). Temperature extremes: Effect on plant growth and development. *Weather Clim. Extremes* **10**:4–10. DOI:10.1016/j.wace.2015.08.001
54. Buira A., Fernández-Mazuecos M., Aedo C., et al. (2021). The contribution of the edaphic factor as a driver of recent plant diversification in a Mediterranean biodiversity hotspot. *J. Ecol.* **109**:987–999. DOI:10.1111/1365-2745.13527
55. Indoria A. K., Sharma K. L. and Reddy K. S. (2020). Chapter 18 - Hydraulic properties of soil under warming climate. In climate change and soil interactions, M.N.V. Prasad, and M. Pietrzykowski, eds. (Elsevier), pp:473-508. DOI:10.1016/B978-0-12-818032-7.00018-7
56. Štraus D., Redondo M. Á., Castaño C., et al. (2024). Plant–soil feedbacks among boreal forest species. *J. Ecol.* **112**:138–151. DOI:10.1111/1365-2745.14224
57. Nimalka Sanjeewani H. K., Samarasinghe D. P. and De Costa W. A. J. M. (2024). Influence of elevation and the associated variation of climate and vegetation on selected soil properties of tropical rainforests across a wide elevational gradient. *CATENA* **237**:107823. DOI:10.1016/j.catena.2024.107823
58. Muscarella R., Kolyaie S., Morton D. C., et al. (2020). Effects of topography on tropical forest structure depend on climate context. *J. Ecol.* **108**:145–159. DOI:10.1111/1365-2745.13261
59. Wang G., Yang L., Wu X., et al. (2025). Density-dependent selection effect of dominant species rather than species diversity increased aboveground biomass accumulation in a temperate oak forest. *For. Ecol. Manage.* **582**:122563. DOI:10.1016/j.foreco.2025.122563
60. Kang H., Xue Y., Cui Y., et al. (2024). Nutrient limitation mediates soil microbial community structure and stability in forest restoration. *Sci. Total Environ.* **935**:173266. DOI:10.1016/j.scitotenv.2024.173266
61. Spohn M. and Stendahl J. (2024). Soil carbon and nitrogen contents in forest soils are related to soil texture in interaction with pH and metal cations. *Geoderma* **441**:116746. DOI:10.1016/j.geoderma.2023.116746
62. Iroshaka Gregory Marcelus Cooray P. L., Chalmers G. and Chittleborough D. (2025). A review of properties of organic matter fractions in soils of mangrove wetlands: Implications for carbon storage. *Soil Biol. Biochem.* **201**:109660. DOI:10.1016/j.soilbio.2024.109660
63. Van Sundert K., Horemans J. A., Stendahl J., et al. (2018). The influence of soil properties and nutrients on conifer forest growth in Sweden, and the first steps in developing a nutrient availability metric. *Biogeosciences* **15**:3475–3496. DOI:10.5194/bg-15-3475-2018
64. Pan Y., Fan Y., Chen C., et al. (2024). Does soil nutrient heterogeneity affect the competition and adaptation of Vernicia montana. *For. Ecol. Manage.* **561**:121877. DOI:10.1016/j.foreco.2024.121877
65. Russo S. E., Davies S. J., King D. A., et al. (2005). Soil-related performance variation and distributions of tree species in a Bornean rain forest. *J. Ecol.* **93**:879–889. DOI:10.1111/j.1365-2745.2005.01030.x
66. Zhang B., Jackson T. D., Coomes D. A., et al. (2025). Soils and topography drive large and predictable shifts in canopy dynamics across tropical forest landscapes. *New Phytol.* **247**:1666–1679. DOI:10.1111/nph.70300
67. Tao S., Guo Q., Li C., et al. (2016). Global patterns and determinants of forest canopy height. *Ecology* **97**:3265–3270. DOI:10.1002/ecy.1580
68. Murphy B. A., May J. A., Butterworth B. J., et al. (2022). Unraveling forest complexity: Resource use efficiency, disturbance, and the structure-function relationship. *J. Geophys. Res-biogeo.* **127**:e2021JG006748. DOI:10.1029/2021JG006748
69. Jiang S., Zhao P., Ma Q., et al. (2025). Evidence of threat from short-timescale dry season drought on tree radial growth in China's humid subtropical forest. *Agric. For. Meteorol.* **373**:110744. DOI:10.1016/j.agrformet.2025.110744
70. Su J., Gou X., HilleRisLambers J., et al. (2021). Increasing climate sensitivity of subtropical conifers along an aridity gradient. *For. Ecol. Manage.* **482**:118841. DOI:10.1016/j.foreco.2020.118841
71. Njoroge B., Li Y., Otieno D., et al. (2022). Seasonal droughts drive up carbon gain in a subtropical forest. *J. Plant Ecol.* **16**:Page–range. DOI:10.1093/jpe/rtac088
72. Laflower D. M., Hurteau M. D., Koch G. W., et al. (2016). Climate-driven changes in forest succession and the influence of management on forest carbon dynamics in the Puget Lowlands of Washington State, USA. *For. Ecol. Manage.* **362**:194–204. DOI:10.1016/j.foreco.2015.12.015
73. Campbell J. L., Driscoll C. T., Jones J. A., et al. (2022). Forest and freshwater ecosystem responses to climate change and variability at US LTER Sites. *BioScience* **72**:851–870. DOI:10.1093/biosci/biab124
74. Grimm N. B., Chapin III F. S., Bierwagen B., et al. (2013). The impacts of climate change on ecosystem structure and function. *Front. Ecol. Environ.* **11**:474–482. DOI:10.1890/120282
75. Xie Y., Wang X. and Silander J. A. (2015). Deciduous forest responses to temperature, precipitation, and drought imply complex climate change impacts. *Proc. Natl. Acad. Sci. USA* **112**:13585–13590. DOI:10.1073/pnas.1509991112
76. Gu H., Qiao Y., Xi Z., et al. (2022). Warming-induced increase in carbon uptake is linked to earlier spring phenology in temperate and boreal forests. *Nat. Commun.* **13**:3698. DOI:10.1038/s41467-022-31496-w
77. Zhang X., Rademacher T., Liu H., et al. (2023). Fading regulation of diurnal temperature ranges on drought-induced growth loss for drought-tolerant tree species. *Nat. Commun.* **14**:6916. DOI:10.1038/s41467-023-42654-z
78. Zhao F., Shi W., Xiao J., et al. (2025). Recent weakening of carbon-water coupling in northern ecosystems. *npj Clim. Atmos. Sci.* **8**:161. DOI:10.1038/s41612-025-01059-z
79. Cui J., Deng O., Zheng M., et al. (2024). Warming exacerbates global inequality in forest carbon and nitrogen cycles. *Nat. Commun.* **15**:9185. DOI:10.1038/s41467-024-53518-5
80. Foster D., Swanson F., Aber J., et al. (2003). The importance of land-use legacies to ecology and conservation. *BioScience* **53**:77–88. DOI:10.1641/0006-3568(2003)053[0077:Tiolul]2.0.Co;2
81. Perring M. P., De Frenne P., Baeten L., et al. (2016). Global environmental change effects on ecosystems: The importance of land-use legacies. *Global Change Biol.* **22**:1361–1371. DOI:10.1111/gcb.13146
82. Schimel D., Pavlick R., Fisher J. B., et al. (2015). Observing terrestrial ecosystems and the carbon cycle from space. *Global Change Biol.* **21**:1762–1776. DOI:10.1111/gcb.12822
83. Yang Q., Niu C., Liu X., et al. (2023). Mapping high-resolution forest aboveground biomass of China using multisource remote sensing data. *GISci. Remote Sens.* **60**:2203303. DOI:10.1080/15481603.2023.2203303
84. Liu A., Cheng X. and Chen Z. (2021). Performance evaluation of GEDI and ICESat-2 laser altimeter data for terrain and canopy height retrievals. *Remote Sens. Environ.* **264**:112571. DOI:10.1016/j.rse.2021.112571
85. Dietze M. C., Fox A., Beck-Johnson L. M., et al. (2018). Iterative near-term ecological forecasting: Needs, opportunities, and challenges. *Proc. Natl. Acad. Sci. USA* **115**:1424–1432. DOI:10.1073/pnas.1710231115

86. Walker L. R., Wardle D. A., Bardgett R. D., et al. (2010). The use of chronosequences in studies of ecological succession and soil development. *J. Ecol.* **98**:725–736. DOI:10.1111/j.1365-2745.2010.01664.x

FUNDING AND ACKNOWLEDGMENTS

This work was supported by the National Natural Science Foundation of China (32501468, 42371329) and the Key Program of the National Natural Science Foundation of China (42530503). The funders had no role in study design, data collection and analysis, decision to publish, or preparation of the manuscript.

AUTHOR CONTRIBUTIONS

K. C. and Q. G. conceived the study. K. C., A. C., and Y. Z. designed the methodology. K. C. drafted the manuscript, with review and editing contributions from Q. G., A. C., and Y. Z. K. C. and Q. G. secured the funding. Q. G. supervised the work and provided resources. All authors contributed to the manuscript and approved the final version.

DECLARATION OF INTERESTS

The authors declare no competing interests.

DATA AND CODE AVAILABILITY

The dataset used in this study was all publicly available. The details are as follows: (1) spatial distribution dataset of natural forest restoration (https://doi.org/10.5281/zenodo.1489322), (2) CSC dataset (https://developers.google.com/earth-engine/datasets/catalog/LARSE_GEDI_GEDI02_B_002_MONTHLY?hl=zh-cn#bands), (3) AGBD dataset (https://developers.google.com/earth-engine/datasets/catalog/LARSE_GEDI_GEDI04_B_002?hl=zh-cn), (4) Climate dataset (https://worldclim.org/data/index.html), (5) Topography dataset (https://earthexplorer.usgs.gov/), (6) Soil dataset (https://www.tpdc.ac.cn/zh-hans/data/e1ccd22c-348f-41a2-ab46-dd1a8ac0c955/). All original code has been deposited at figshare and is publicly available at https://doi.org/10.6084/m9.figshare.30280561.v1.

SUPPLEMENTAL INFORMATION

It can be found online at https://doi.org/10.59717/j.xinn-geo.2026.100228.